Material Modeling and Experimental Study of Serrated Chip Morphology

T. Mabrouki[a], L. Deshayes[b], R. Ivester[b], J.-F. Rigal[a], K. Jurrens[b]
[a]INSA-LYON, Domaine scientifique de la Doua
Laboratoire LaMCoS , Bât. Joseph Jacquard

[b] NIST Manufacturing Engineering Laboratory
Gaithersburg, Maryland USA

Abstract
Machining chip morphology stems from mechanical, thermal, and chemical phenomena. Chip morphology prediction depends on a fundamental understanding of these phenomena and is industrially important for cutting force prediction and surface integrity control. Our paper focuses on modeling serrated-chip formation through comparison of thermo-mechanical simulations of cutting processes to experimental observations. The simulations utilize plasticity and damage models to predict chip morphology. The major points treated in this paper concern physical phenomena accompanying serrated-chip formation with variation of feed. Experimental analysis of chip morphology supports simulation results for various cutting parameters and American Iron and Steel Institute (AISI) 4340 steel.

Keywords: Finite Element Method, Machining, Chip Morphology

1 INTRODUCTION

In order to develop a new cutting process and to reduce time and resource costs, it is necessary to determine the optimal range of the cutting parameters. Selection of cutting parameters such as tool geometry, cutting speed and feed rate directly influence the interactions at the tool-chip interface [1] and consequently the chip morphology. Moreover, the tool-chip interface is the excitation element for the dynamic behavior of the machining system, so these interactions also affect the dynamics of the cutting process [2-4]. Experimental approaches to determine optimal cutting parameters are very widespread. The CWT (Couple Workpiece Tool) methodology [5] is used to obtain such parameters with a minimum of experiments [1]. Nevertheless these experiments are always costly due to the need for specialized equipment such as dynamometers, accelerometers, and data acquisition systems. Generally a complete CWT is realized when, for a given cutting process, it is necessary to determine ranges of cutting parameters for achieving a given quality criteria or cost function.

Computer simulations of the cutting process complement the experimental approach by minimizing the number of design iterations and reducing design cost. Unfortunately, few valid physics-based models are available due to the high strain rate during chip formation and the mechanical, thermal, and metallurgical complexity of the tool-workpiece interactions. However, numerical studies are increasingly present through scientific publications [6-9] in the last decade. Due to increasing interest in high-speed machining and hard turning, investigations of chip formation with high cutting speeds and hard materials have appeared [10-12]. Consequently, cutting speed has been the primary parameter studied for chip formation simulation. Few numerical studies have been made concerning the chip formation according to feed rate.

In conventional machining practice, the determination of valid ranges for depth of cut, *ap*, and feed rate, *f*, is critical for the choice of cutting parameters for a given combination of workpiece and tool materials. Such determinations are generally made through experiments or handbook data. Due to the tool-chip interface complexity, caused by the increasing importance of complex chip breaker geometries and tool coatings, it is not easy to obtain satisfactory results by numerical simulations. Preliminary studies [1] [13] have shown that for American Iron and Steel Institute (AISI) 4340 steel, the feed range corresponds to a shear-localized chip formation. The shear-localized chips are also called saw-tooth chips, or serrated chips. They have been observed in machining different materials, such as AISI 4340 steel [13], Titanium [14] and its alloys [15]

and Nickel Iron based super alloys [16]. Nevertheless, one of the most difficult problems to solve is to determine exactly the feed value for which the transition from continuous to serrated chip occurs.

The focus of this paper is on comparison of oblique cutting experimental observations to Finite Element Modeling (FEM) simulations. Two FEM simulations are compared: a modeling approach using a strain-rate and temperature dependent elasto-visco-plastic material model, and a simulation for which the chip is modeled with a damage model. In the next section, first we propose a brief review on chip formation theory and then we present experimental results of chip formation according to feed rate. In section 3 we describe the finite element models used for the simulations. In section 4 we compare numerical results performed with the ABAQUS/EXPLICIT[1] code and Thirdwave Systems' Advantedge[1] with those obtained experimentally. The paper ends with further discussions and concluding remarks.

2 CHIP FORMATION AND EXPERIMENTAL OBSERVATIONS

2.1 Brief Review on Chip Formation

The study of chip formation began in the 1930s and 1940s, based on the work of Taylor [17] and Mallock [18]. Since then, various scientists have made different chip classifications, including Ernst [19], Shaw [20], Recht [21], Rice [22], and Davies [11]. Komanduri [23] and Davies [10] have presented relevant review papers considering conventional machining operations. Figure 1 presents the main chip types considered in our study. Continuous chips (Figure 1a) are considered to be non-oscillatory material flow in which profiles of chip properties (strain, stress, temperatures...) remain approximately constant over time. Figure 1b shows a segmented chip that is a continuous chip in which shear zones appear aperiodically and chip thickness varies with time. Some authors [24] explain that this type of chip morphology appears due to stick-slip oscillation and damage in the shear zone. Shaw [20] identified serrated or shear-localized chips (Figure 1c) and characterized them as oscillatory material flow. This oscillatory phenomenon has been widely modeled in hard turning by authors such as Davies and Burns [10]. Finally, discontinuous chips can be obtained when chip segmentation increases to the point where each segment breaks as shown in Figure 1d. Field and Merchant [25] have shown that in the case of machining bronze alloys, the periodic rupture appears in the shear zone and could be due to oscillatory compressive stress occurring from the tool tip and propagating toward the free chip surface. For steel alloys, such as AISI 4340, other researchers [1,13] have observed that the chip fracture seems to propagate from the free surface towards the tool tip.

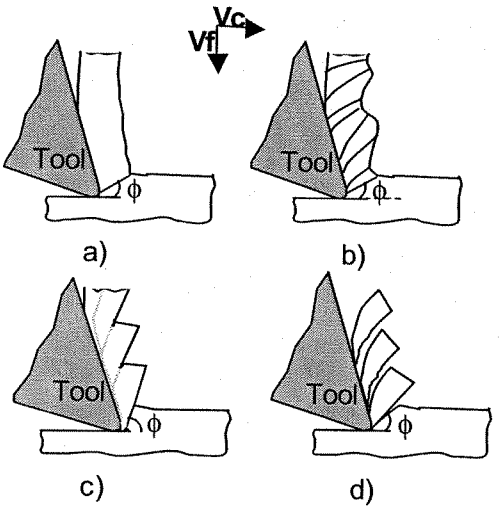

Figure 1: Different chip types produced during a turning operation: (a) continuous; (b) segmented; (c) serrated or sheared localized; (d) discontinuous.

In practice, manufacturers need a two dimensional diagram representing valid ranges for feed and depth of cut for a given combination of tool and workpiece material, referred to as a "fragmentation diagram" in the CWT methodology [1,5]. For a given tool and workpiece material, the fragmentation diagram represents the feed and depth of cut ranges that result in segmented chip formation. Figure 2 shows a general 2D fragmentation diagram whose borders are defined by different criteria. The minimum feed defines the left part of the diagram. For an insert with simple chip-breaker geometry, the minimum feed does not depend on the depth of cut. For more complex insert geometries, this border depends on both feed

[1] Commercial equipment and materials are identified in order to adequately specify certain procedures. In no case does such identification imply recommendation or endorsement by the National Institute of Standards and Technology, nor does it imply that the materials or equipment are necessarily the best available for the purpose. Official contribution of the National Institute of Standards and Technology; not subject to copyright in the United States.

rate and depth of cut. The bottom border of this diagram corresponds to the minimum depth of cut, ap_{min}, for the given insert geometry. The determination of ap_{min} depends on the tool breaker geometry in the area of the tool nose and the nose radius. This border is not influenced by the feed rate. The upper diagram border, limited by ap_{max}, and the right border, f_{max}, represents the maximum depth and feed admissible by the tool to avoid short tool life or machining instability. Then machine limits and surface quality criteria will limit the upper right zone of the diagram. Generally, these limits can be obtained by using tool provider or handbook recommendations. At significantly higher cost, the diagram can be validated through experiments and analysis of chip aspects, specific cutting forces, surface quality and process stability.

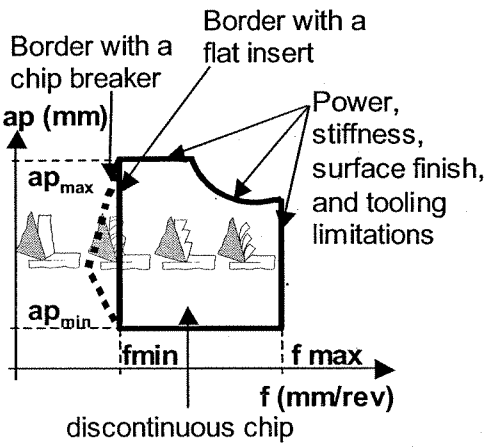

Figure 2: Fragmentation diagram

Our study focuses on chip formation with increasing feed rate. Experiments [1] show that a transition takes place from continuous to shear localized and discontinuous chips when feed increases, as shown in Figure 2. The following section focuses on this transition.

2.2 Experimental Observations

In this section we present experimental evidence of chip transition morphology from continuous to serrated chip. The transition to shear-localized chip formation when cutting speed increases has been demonstrated by various authors and for distinct materials. However, few studies have been made concerning this transition when feed rate increases. In our study we consider an AISI 4340 steel alloy with a hardness of 38.9 HRC.

Experiments have been conducted on a SOMAB 400 20 kW numerically controlled lathe and cutting forces have been measured with a three-dimensional force transducer. Two different insert geometries have been considered, with mean values as given in the left part of Figure 3. A flat negative rake angle insert and a more complex positive rake angle insert have been used. Depth of cut and cutting speed were fixed at 2 mm and 120 m/min respectively for all experiments. The cutting speed value has been chosen to be close to the maximum cutting speed acceptable for this combination of tool and workpiece material (CWT). Experiments were conducted with feed values from 0.05 mm/rev to 0.4 mm/rev.

To obtain a chip type number representing the macro structure chip morphology, chips were

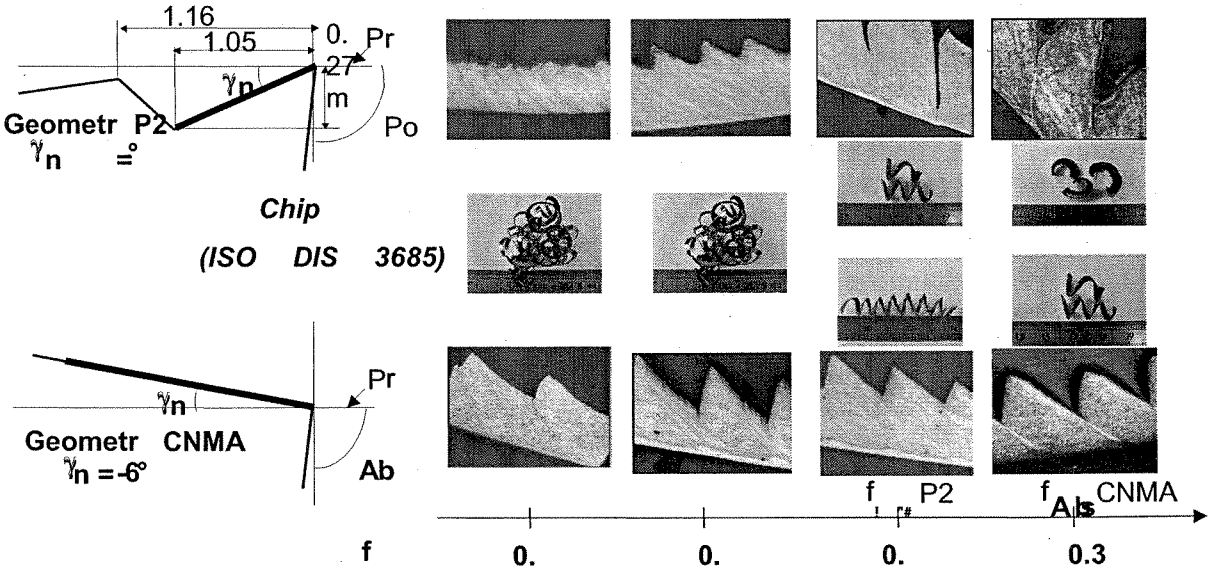

Figure 3: Chip morphology evolution with feed rate for two chip breaker geometries (P2 and CNMA) and with ap = 2mm, Vc = 120 m/min

collected for each feed value and were compared to those given in ISO 3685 [26]. Figure 3 presents the main chip types observed during the experiments. In the CWT methodology, 4.2 and 6.2 chip types are considered as acceptable chips for determining the range of acceptable values for feed. 6.2 chip types are the first acceptable chips appearing as feed increases. Consequently f_{min} corresponds to the feed value for which this chip type first appears. The minimum value of feed for tools P2 and CNMA are 0.3 mm/rev and 0.35 mm/rev respectively.

In order to analyze the chip morphology completely, the chips must be cross-sectioned, polished, etched in 4% nitric acid in ethyl alcohol and examined under a microscope. Figure 3 presents results of this process. For tool P2 we observe that the chip characteristics evolution is from continuous to serrated chips exactly as in Figure 2. Other experiments made by Komanduri [13] have shown that it is also possible to obtain discontinuous chips for higher cutting speed or higher feed rates. For the negative tool CNMA, we observe that the chip morphology transitions from serrated continuous chips to shear localized chips. The minimum feed rates for these two tools (f_{min}P2 and f_{min}CNMA) seem to correspond to a shear localized chip.

Figure 4 shows typical results for two different feed rates. Figure 4a illustrates a serrated continuous chip with a feed rate of 0.224 mm/rev, lower than f_{min} for this tool. This micrograph shows the chip segment with a width of dc = 0.14 mm, and two zones: a high plastic strain shear band zone with a width of Sb = 0.06 mm, and a zone with very little plastic strain. As the feed rate increases, the shear band zone becomes narrower and is typically called an adiabatic shear band. This is observed in Figure 4b for a feed of 0.35 mm/rev (greater than f_{min}) where it is noted that a crack appears on the free side of the chip along the shear band. This band occurs because of a combination of high plastic deformation due to localized material softening and damage that facilitates fracture along this plane. We can observe that the width of the shear band is becoming larger from the free chip surface to the tool tip. At the free chip surface, the width of the shear band is about 0.01 mm, and at the tool tip side it is about 0.1 mm. The width of the shear band at the tip interface depends mainly on the tool tip radius, which measured 50 µm for tools CNMA and P2. This large zone allows crack formation and consequently cracks propagation and fractures along the shear plane. Moreover for higher feeds and cutting speeds, fractures can be observed [13] to increase.

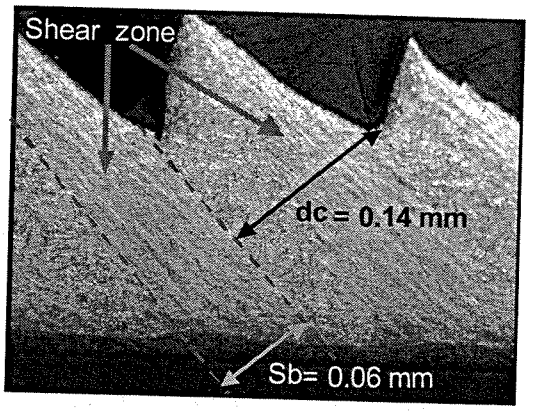

(a)

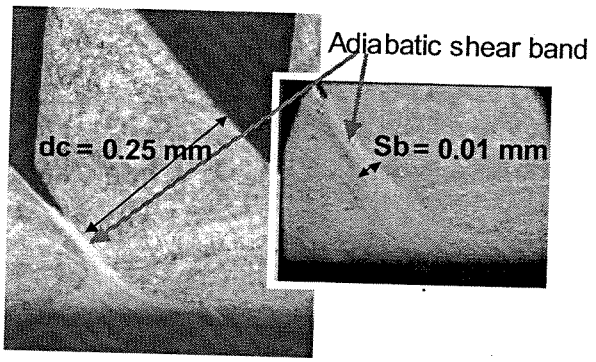

(b)

Figure 4: Photography of chip microstructure obtained with the flat tool CNMA and AISI 4340 machined steel alloy with: (a) f=0.224 mm/rev, (b) f = 0.35 mm/rev.

In the primary shear zone, these experimental observations clearly identify that the transition from a serrated continuous chip to a shear-localized chip is governed by high plastic deformation of the material and by material damage. In the remainder of this paper, we analyze physical phenomena accompanying shear localized chip formation using FEM simulations.

3 FINITE ELEMENT MODEL

To simulate chip formation, it is necessary to establish an appropriate separation criterion to permit the tool tip movement and a realistic relation between chip morphology and cutting parameters. This criterion must be in agreement with the physics of shear-localized chip formation. Some authors claim that the chip formation process is carried out only by

plastic deformation. According to them, the chip formation can be simulated by plastic flow. Consequently, the separation of the chip from the workpiece in a FEM simulation can be achieved by continuous re-meshing [27]. Other authors have used separation criteria based on critical strain energy [28] or on de-bonding surfaces [8]. The most suitable criterion is that which closely represents the physics of tool-workpiece interaction, as determined through comparison to experiments.

In order to model the case of orthogonal cutting in ABAQUS/EXPLICIT, ABAQUS/CAE [30] has been used for pre-processing, where the workpiece mechanical and thermal properties, contact conditions between the tool and machined workpiece, and boundary conditions have been defined. The resulting input file is processed and sent to ABAQUS/EXPLICIT to perform coupled temperature-displacement calculations. The cutting modeling uses four-node bilinear displacement and temperature (CPE4RT) quadrilateral elements with a plane strain assumption in both the workpiece and the cutting tool. An Arbitrary Lagrangian Eulerian (ALE) technique describes the relative motions between the chip, tool, and workpiece. Because machining is an extremely dynamic event with large changes in geometry occurring over a relatively small number of increments, it was necessary to increase the frequency and intensity of adaptive meshing. Figure 5 illustrates the mesh of the orthogonal cutting model used in ABAQUS (entering angle χ = 90°, a cutting speed V_C = 120 m/min, feed levels of f = 0.22 mm/rev. Rake face is fixed to γ = -6°and flank (or clearance) angle is α = 5°.

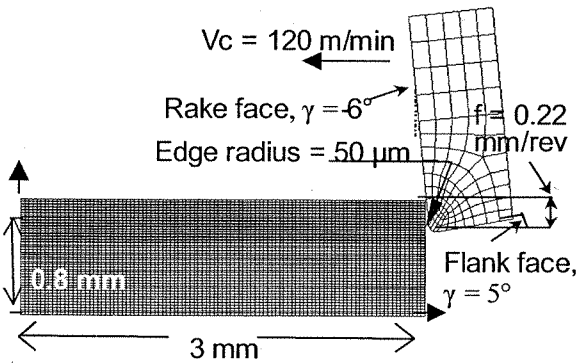

Figure 5: ABAQUS geometric cutting model

The Advantedge simulations were performed using its adaptive re-meshing scheme as documented in [29]. The tool geometry and cutting parameters used for Advantedge were identical to those used in ABAQUS/EXPLICIT.

3.1 Material model and tool data

For the material behavior of the machined workpiece (AISI 4340), a Johnson-Cook model [31] was used for ABAQUS/EXPLICIT and the default material model was used in Advantedge. The Johnson-Cooke model is a strain-rate and temperature dependent visco-plastic material model suitable for problems where strain rates vary over a large range (10^2 s^{-1} - 10^6 s^{-1}), and temperature changes due to plastic deformation caused by thermal softening. This model represents the equivalent flow stress as the following equation:

$$\bar{\sigma} = \underbrace{\left(A + B\bar{\varepsilon}^{n}\right)}_{\substack{Elasto-plastic \\ term}} \underbrace{\left[1 + C\ln\left(\frac{\dot{\bar{\varepsilon}}}{\dot{\bar{\varepsilon}}_0}\right)\right]}_{\substack{Viscosity \\ term}} \underbrace{\left[1 - \left(\frac{T - T_{room}}{T_{melt} - T_{room}}\right)^{m}\right]}_{\substack{Softening \\ term}} \quad (1)$$

Where $\bar{\sigma}$ is equivalent stress, $\bar{\varepsilon}$ equivalent strain, $\dot{\bar{\varepsilon}}$ plastic strain rate, $\dot{\bar{\varepsilon}}_0$ reference strain rate ($1.0\ s^{-1}$), T_{room} room temperature, and T_m melting temperature.

These five constants *A, B, n, C* and *m,* were determined from experimental tests [8]. Where *A* is the initial yield stress *[MPa], B* is the hardening modulus, *n* is the work-hardening exponent, *C* is the strain rate dependency coefficient *[MPa]*, and *m* is the thermal softening coefficient. The parameter values used in modelling the AISI 4340 workpiece and the cutting tool are specified in Tables 1 - 2.

A (Mpa)	B (MPa)	n	C	m
910	586	0.26	0.014	1.03

Table 1: Johnson-Cook parameters [33].

Thermal Parameter	Workpiece	Tool
Density ρ *(Kg/m^3)*	7850	11900
Elastic modulus *E (GPa)*	205	534
Poisson's ratio *v*	0.3	0.22
Specific heat C_p *(Jkg^{-1}°C^{-1})*	475	400
Thermal conductivity λ *(W.m^{-1}°C^{-1})*	44.5	50
Expansion *(µm.m^{-1}°C^{-1})*	13.7	×
T_{melt} *(°C)*	1520	×
T_{room} *(°C)*	25	25

Table 2: Workpiece and tool thermal parameters.

3.2 Chip formation modeling

In the two simulation environments discussed in this paper, we have modeled material behavior in two different ways in order to produce chip segmentation. For the simulations

in ABAQUS/EXPLICIT, a fracture damage model evokes chip segmentation behavior. In Advantedge, a very fine mesh (~2 micrometer minimum mesh element size) together with thermal softening evokes chip segmentation behavior. The fracture damage in ABAQUS/EXPLICIT is modeled according to a cumulative damage law.

$$D = \sum \left(\frac{\Delta \bar{\varepsilon}}{\bar{\varepsilon}_f} \right) \tag{2}$$

In this cumulative damage law $\Delta\bar{\varepsilon}$ represents the equivalent strain increment. The cumulative strain $\Delta\bar{\varepsilon}$ is updated at every analysis increment. $\bar{\varepsilon}_f$ is the equivalent failure strain and is expressed as the following equation :

$$\bar{\varepsilon}_f = \left[D_1 + D_2 \exp\left(D_3 \frac{P}{\sigma_{eff}} \right) \right] \times \left[1 + D_4 \ln\left(\frac{\dot{\bar{\varepsilon}}}{\dot{\bar{\varepsilon}}_0} \right) \right] \times \left[1 + D_5 \left(\frac{T - T_{romm}}{T_{melt} - T_{room}} \right) \right] \tag{3}$$

where $\bar{\varepsilon}_f$ depends on the ratio $\dot{\bar{\varepsilon}} / \dot{\bar{\varepsilon}}_0$, the equivalent strain $\dot{\bar{\varepsilon}}$, the ratio of hydrostatic pressure to effective stress P / σ_{eff}, and the temperature. It also depends on the damage constants (D_i, $1 \le i \le 5$), which are determined experimentally [8]. The failure of elements is assumed to occur when $D = 1$. The damage constants of AISI 4340 standard alloy steel [32] are presented in the Table 3.

Work material	D_1	D_2	D_3	D_4	D_5
AISI 4340	-0.80	2.10	-0.50	0.002	0.61

Table 3: Cumulative damage law parameters.

3.3 Tool/chip interaction

Modeling of tool-chip friction in ABAQUS/EXPLICIT was based on Coulomb's friction law. This manner of friction modeling has been used in several previous publications [33, 34]. This law is defined by equations (4, 5) where $\bar{\tau}$ is the shear flow stress of the chip, μ friction coefficient, and σ_n is the normal stress along the tool rake face. Sticking or sliding frictional conditions along the tool/chip interface are dependent on stress magnitude.

- $\bar{\tau} = \mu\sigma_n$, $\mu\sigma_n \le \bar{\tau}_{max}$ (sliding region) (4)
- $\bar{\tau} = \bar{\tau}_{max}$, $\mu\sigma_n \ge \bar{\tau}_{max}$ (sticking region) (5)

We have assumed that the friction coefficient is equal to a mean value of 0.2 and $\bar{\tau}_{max}$ is given by equation (6).

$$\bar{\tau}_{max} = \frac{A}{\sqrt{3}} \tag{6}$$

3.4 Heat generation

The heat generated during cutting is the result of plastic deformation and friction. If we consider a local temperature rise of ΔT_p in the workpiece during a period of time Δt, the heat generation rate $\dot{q}_P$ due to inelastic work is given by the equation (7):

$$\dot{q}_P = \rho C_p \frac{\Delta T_P}{\Delta t} = \eta_p \sigma_{eff} \dot{\varepsilon} \tag{7}$$

Where η_P is the fraction of inelastic heat (it is assumed that $\eta_P = 0.90$ [33, 34]). The heat generated by friction is due to a rise temperature ΔT_f during a period time of Δt due to friction forces. According to references [33, 34], the fraction of dissipated energy η_f caused by friction is equal to 1. The corresponding volumetric heat flux $\dot{q}_f$ is shared between work-piece and cutting tool. The fraction of heat going into the tool is calculated by assuming that the bulk temperature in the tool is equal to that in the workpiece. Also, the chip slip velocity is assumed to be similar to that of the cutting tool. So the shearing coefficient is assumed to be as J ≈ 0.5. As a result, heat flux $\dot{q}_f$ is:

$$\dot{q}_f = \rho C_p \frac{\Delta T_f}{\Delta t} = \eta_f J \, \bar{\tau} \, \dot{\gamma} \tag{8}$$

The shear stress $\bar{\tau}$ is given by Coulomb's law, and $\dot{\gamma}$ is the slip strain rate. Consequently, Equation 9 gives the energy equation defining the temperature field.

$$\lambda \nabla^2 T - \rho C p \frac{\Delta T}{\Delta t} + \dot{q} = 0 , \tag{9}$$

where $\dot{q} = \dot{q}_P + \dot{q}_f$.

4 RESULTS AND DISCUSSION

In this section, numerical results dealing with von Mises equivalent stresses, equivalent strains, and temperatures during serrated chip formation are presented. In the simulations using ABAQUS/EXPLICIT, the Johnson-Cook damage model sets the deviatoric stress components to zero for the remainder of the simulation. Therefore, the damage locations are easily seen in the von Mises stress profiles.

In the simulations using Advantedge, the localized thermal softening results in substantially lower stresses around the shear-localized regions. Therefore, the shear banding is also apparent in the von Mises stress profiles for those simulations.

4.1 Results with ABAQUS/EXPLICIT

Figure 6 shows the distribution of equivalent von Mises stresses during workpiece-tool interaction at a time of 0.20 ms. The high magnitude stresses are localized in the primary shear zone and the tool tip zone. Locations with zero stress levels represent damaged zones in the chip.

Figure 7 shows the distribution of the equivalent strains generated during tool-workpiece interaction corresponding to a machining time of 0.20 ms. It is noted that strains as high as 1.96 occur. In general, the highest strains occur along the primary and secondary shear zones. Consequently, temperature values in these regions increase, as shown in Figure 8.

The high shear stress along the primary shearing zone causes higher strains and results in material damage. This inelastic behavior occurs at the tool tip and is propagated along the primary shear zone. This causes a plastic deformation and localized heating, resulting in thermal softening (Figure 8). The von Mises results suggest that a micro-crack can initiate at the tool tip zone and propagate along the primary shear zone. A second micro-crack can accompany the first one, initiating on the free side of the chip and propagating along the primary shear zone towards the tool tip. If either of these micro-cracks occurs and penetrates through the entire chip, or if these two micro-cracks occur and intersect, the chip becomes discontinuous as in Figure 1d.

Figure 9 shows the evolution of cutting force as time function. It is observed that when the crack appears the force decreases by 35 %.

4.2 Results with Advantedge

Simulations were conducted in Thirdwave Systems' Advantedge for two conditions corresponding to cutting conditions of actual experiments presented in section 2. Cutting parameters for the first simulation were 120 m/min cutting speed and 0.4 mm/rev feed. Cutting parameters for the second simulation were 120 m/min cutting speed and 0.22 mm/rev feed. This section presents results from those simulations.

Figures 10, 11, and 12 show the workpiece and tool–chip interface distributions of von Mises stresses, plastic strains, and temperatures, respectively, for the simulation with 0.4 mm/rev feed. In Figure 10, The von Mises stresses are highest at the tool tip and surrounding the primary shear zone. The center of the primary shear zone has very low stresses due to thermal softening caused by shear localization. In Figure 11, the plastic strains are highest along the tool-chip interface and at locations where shear localization occurs. As is evident in part of the chip, this shear localization appears to be periodic. The separation between the shear-localized bands corresponds very closely to measurements from analysis of chips from experiments as shown in Figure 4b. In Figure 12, the temperatures are highest along the tool-chip interface and in the area of shear localization.

Figure 13, 14, and 15 show the workpiece and tool–chip interface distributions of von Mises stresses, plastic strains, and temperatures, respectively, for the simulation with 0.22 mm/rev feed. These locations of high and low values of von Mises stress, plastic strain, and temperature, are similar to those in Figures 10–12.

The key differences between the profiles in Figures 10-12 and Figures 13-15 are the separation between shear localization bands most evident in Figures 11 and 14. In close correlation to the experimental results in Figure 4a and 4b, the separation between the shear bands increases with feed rate.

4.3 Comparison of simulation results with experimental observations

In terms of the chip morphology and cutting and thrust forces, the experimental results can be compared to the simulation results. The cutting and thrust forces from the experiments compare very favorably to the simulation forces from Advantedge in terms of cutting force per unit width of cut in Tables 4 and 5. The chip thickness, width of the shear band, and shear band separation values are also very similar, as can be seen in Tables 4 and 5.

Concerning specific cutting force results with ABAQUS/EXPLICIT, significant differences with experimental ones are noted. However, very close results are obtained concerning the shear band and the segment width. Comparing ABAQUS/EXPLICIT temperature results in

Figure 8 with Advantedge temperature results in Figure 15, we observe some differences between the two simulations on contact length and temperature distributions. Such differences can be explained by different material modeling of the workpiece and tool and modeling friction between the chip and the tool. The difference in material modeling between the two simulations is that the Johnson Cook damage model has been used in ABAQUS/EXPLICIT and a viscoplastic model without material damage has been used for Advantedge.

	ap (mm)	Kct (N/mm²)	Kcc (N/mm²)	Sb (mm)	Dc (mm)
Abaqus	1	1600	2050	0.06	0.20
Advantedge	1	2366	3125	0.05	0.17
Experiments	2	2284	3051	0.06	0.14

Table 4: results comparison with Vc = 120 m/min and f = 0.22 mm/rev.

	ap (mm)	Kct (N/mm²)	Kcc (N/mm²)	Sb (mm)	dc (mm)
Advantedge	1	1750	2750	0.02	0.24
Experiments	2	1771	2437	0.011	0.25

Table 5: results comparison with Vc = 120 m/min and f = 0.4 mm/rev.

This difference clearly shows the importance of using appropriate material modeling and material properties. Many material models and properties exist in the literature, which leads to confusion in interpreting simulation results. Before simulations can be reliable, it is necessary to validate their predictions by conducting experimental work to measure material behavior and cutting performance.

5 CONCLUSION

The present work demonstrates that serrated chip formation can be modeled using simulation software with appropriate material and damage models. It seems that chip segmentation of AISI 4340 is the result of ductile shearing. In addition, experimental observations show that cracks can form in the damaged region. Modeling efforts to fully capture the range of cutting parameters for which chip segmentation occurs continue. Our aim is to develop and validate a predictive numerical model that eliminates the need to perform parametric studies of the cutting process. Future work will focus on obtaining precise material properties from a given material and/or damage model, and the impact of material modelling on computation time.

6 REFERENCES

[1] Deshayes, L., 2003, Cutting Methodology Study, Link between Couple Workpiece Tool and Machine Tool Workpiece System (Méthodologie d'étude de la coupe, liaison entre Couple Outil Matière et Pièce Outil Machine). Ph.D. Thesis, Insa de Lyon, 271 p

[2] Eman, K., Wu, S. M., 1980, A Feasibility of On-Line Identification of Chatter in Turning Operations, Journal of Engineering for Industry, 102: 315-321.

[3] Mehdi, K., Rigal, J. F., Play, D., 2002, Dynamic behavior of a thin-walled cylindrical workpiece during the turning process, Part 1: Cutting process simulation, Journal of Manufacturing Science and Engineering, Transactions of the ASME, V. 124/3:562-568.

[4] Mehdi, K., Rigal, J. F., Play, D., 2002, Dynamic behavior of a thin-walled cylindrical workpiece during the turning process, Part 2: Experimental approach and validation, Journal of Manufacturing Science and Engineering, Transactions of the ASME, 124/3:569-580.

[5] NF E66-520-1, 1997, Working zones of cutting tools – Couple Tool-material – part 1: general presentation, French Standard, ISSN 0335-3931.

[6] Yen, Y-C., Jain A., 2003, T. Altan, A finite element analysis of orthogonal machining using different tool edge geometries, Journal of Material Processing and Technology, In Press, Corrected Proof, Available online, 2 September 2003 (http://www.sciencedirect.com).

[7] Lin, C., Lo, S-P., 1998, A study of deformation of the machined workpiece and tool under different low cutting velocities with an elastic cutting tool, International Journal of Mechanical Sciences, 40/7:663–681.

[8] Zhang, B., Bagchi, A., 1994, Finite element simulation of chip formation and comparison with machining experiment, Journal of Engineering for Industry, *Transaction ASME,* 116/3:289–297.

[9] E. Ceretti, M. Lucchi, T. Altan, 1999, FEM simulation of orthogonal cutting: serrated chip formation, Journal of Materials Processing and Technology, 95/1-3:17-26.

[10] Davies, M. A., Burns, T. J., 2001,

Thermomechanical oscillations in material flow during high-speed machining, Phil. Trans. R. Soc. Lond. A, 359 : 821-846.

[11] Davies, M. A., Chou, T., Evans, C.J., 1996, On chip morphology, Tool Wear and Cutting Mechanics in Finish Hard Turning, Annals of the CIRP, 45/1: 77-82.

[12] Tönshoff, H.K. Arendt, C., Ben Amor, R., 2000, Cutting of Hardened Steel, Keynote Paper, Annals of the CIRP Vol. 49/2, pp 547-565.

[13] Komanduri, R., Schroeder, T., Hazra, J., von Turkovich, B. F., Flom, D. G., 1982, On the catastrophic Shear Instability in High-Speed Machining of an AISI 4340 Steel, Journal of Engineering for Industry, Transaction ASME 104: 121-131.

[14] Gente, A., Hoffmeister, H.-W., 2001, Chip Formation in Machining Ti6Al4V at Extremely High Cutting Speeds, Annals of the CIRP, 50/1: 49-52.

[15] Komanduri, R., Turkovich, B. F., 1981, New Observations on the Mechanism of Chip Formation when Machining Titanium Alloys, Wear, 69: 179-188

[16] Komanduri, R., Schroeder, T. A., 1986, On Shear Instability in Machining a Nickel-Iron Basa Superalloy, Journal of Engineering for Industry, Transaction ASME 108: 93-100

[17] Taylor, F. W., 1907, On the art of cutting metals, Trans. ASME, 28 : 307-326

[18] Mallock, A., 1881, The action of cutting tools, Proc. R. Soc. Lond., 33: 127-139

[19] Ernst, H., 1938, Physics of metal cutting, In Machining of metals, Cleveland, OH: American society for Metals, 1-34

[20] Vyas, A., Shaw, M. C., 1999, Mechanics of saw-tooth chip formation in metal cutting. Journal of Manufacturing Science and Engineering, 121/2: 163-172

[21] Recht, R. F., 1964, Catastrophic thermoplastic shear, ASME Journal of Applied Mechanics, 31:189-193.

[22] Rice, W. C., 1961, The formation of continuous chips in metal cutting, Proc. Inst. Mech. Engrs, Lond., 114:141-174

[23] Komanduri, R., 1993, Machining and Grinding: a historical review of the classical papers, Applied Mechanic Review, 46: 80-132.

[24] Komanduri, R., Brown, R. H., 1981, On the mechanics of chip segmentation in machining, Journal of Engineering for Industry, 103: 33-50

[25] Field, M., Merchant, M. E., 1949, Mechanics of Formation of the Discontinuous Chip in Metal Cutting, Transaction of the ASME, 71: 421-430

[26] ISO 3685, 1993, Tool-life testing with single-point turning tools, TC 29, p. 48

[27] Yen, Y-C., Jain, A., Altan, T., 2003, A finite element analysis of orthogonal machining using different tool edge geometries, Journal of Materials Processing and Technology, In Press, Corrected Proof, Available online 2 September 2003 (http://www.sciencedirect.com).

[28] Lin, Z-C., Lo, S-P., 1998, A study of deformation of the machined workpiece and tool under different low cutting velocities with an elastic cutting tool, International Journal of Mechanical Science, 40:663–81.

[29] Marusich, T. D., Ortiz, M., 1995, Modelling and Simulation of High-Speed Machining, International Journal of Numerical Methods in Engineering, 38/21:3675-3694.

[30] Hibitt, Karlsson, Sorensen, ABAQUS/Explicit Theory and Users, Manuals, 2003, Version 6.3.1.

[31] Johnson, G.R., Cook, W.H., 1985, Fracture characteristics of three metals subjected to various strains, strain rates, temperatures and pressures, Engineering Fracture Mechanics, 21/1: 31-48.

[32] Holmquist, T. J., Templeton, D. W., Bishnoi, K. D., *2001,* Constitutive modeling of aluminium nitride for large strain, high-strain rate, and high-pressure applications, International Journal of Impact Engineering, 25/3:211-231.

[33] Nga, E. G., Aspinwall, D.K., Brazil, D., Monaghan, J., 1999, Modelling of temperature and forces when orthogonally machining hardened steel, International Journal of Machine Tools & Manufacture 39: 885–903.

[34] Li, K., Gao, X. -L., Sutherland, J. W., 2002, Finite element simulation of the orthogonal metal cutting process for qualitative understanding of the effects of crater wear on the chip formation process, Journal of Material Processing and Technology, 127/3:309-324.

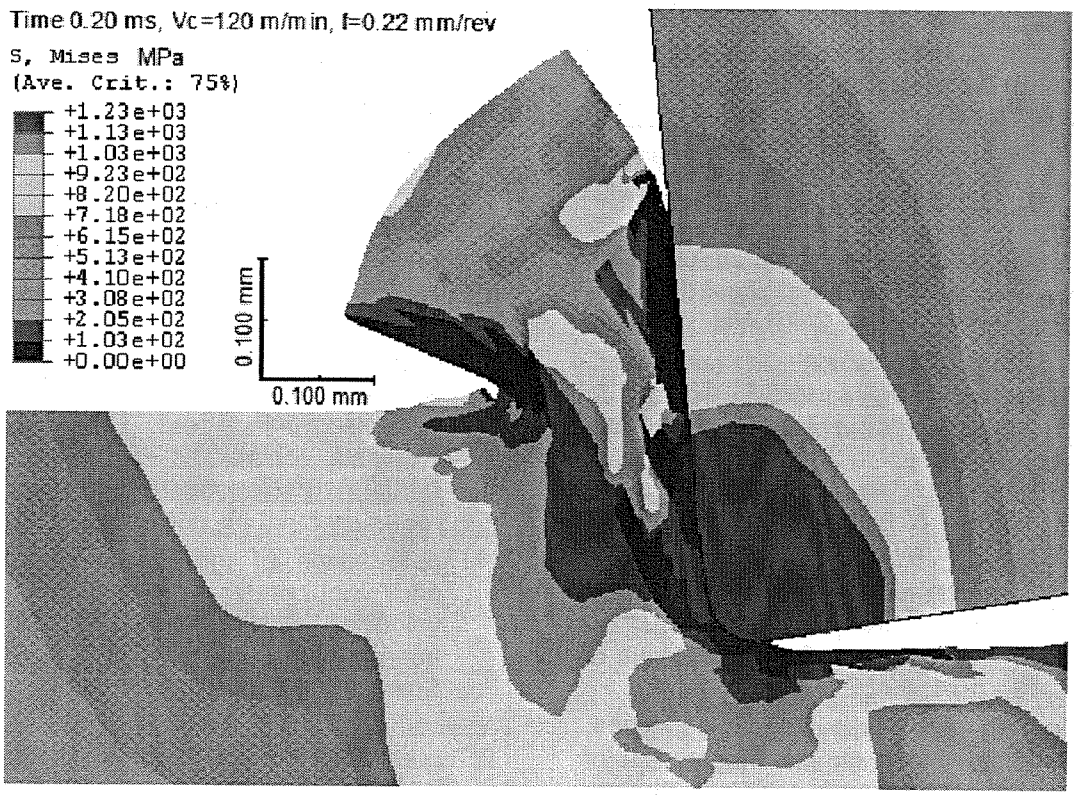

Figure 6: Von Mises equivalent stresses simulation results with ABAQUS

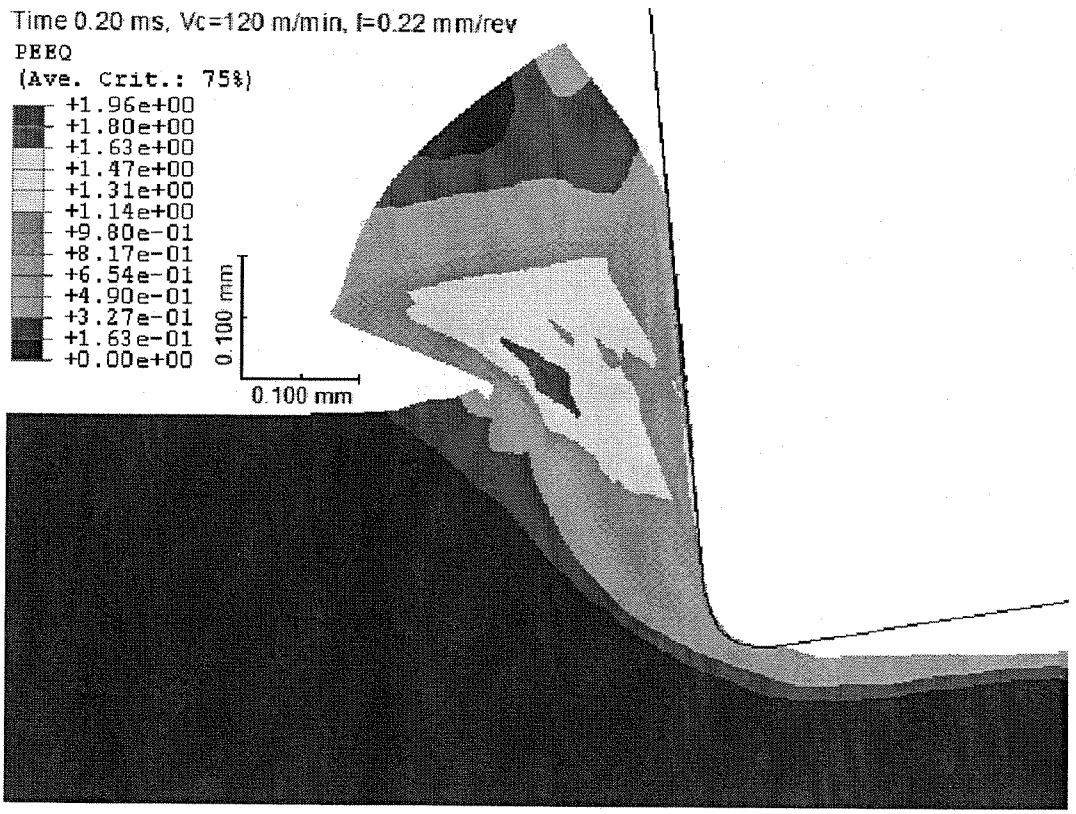

Figure 7: Von Mises equivalent plastic strains simulation results with ABAQUS

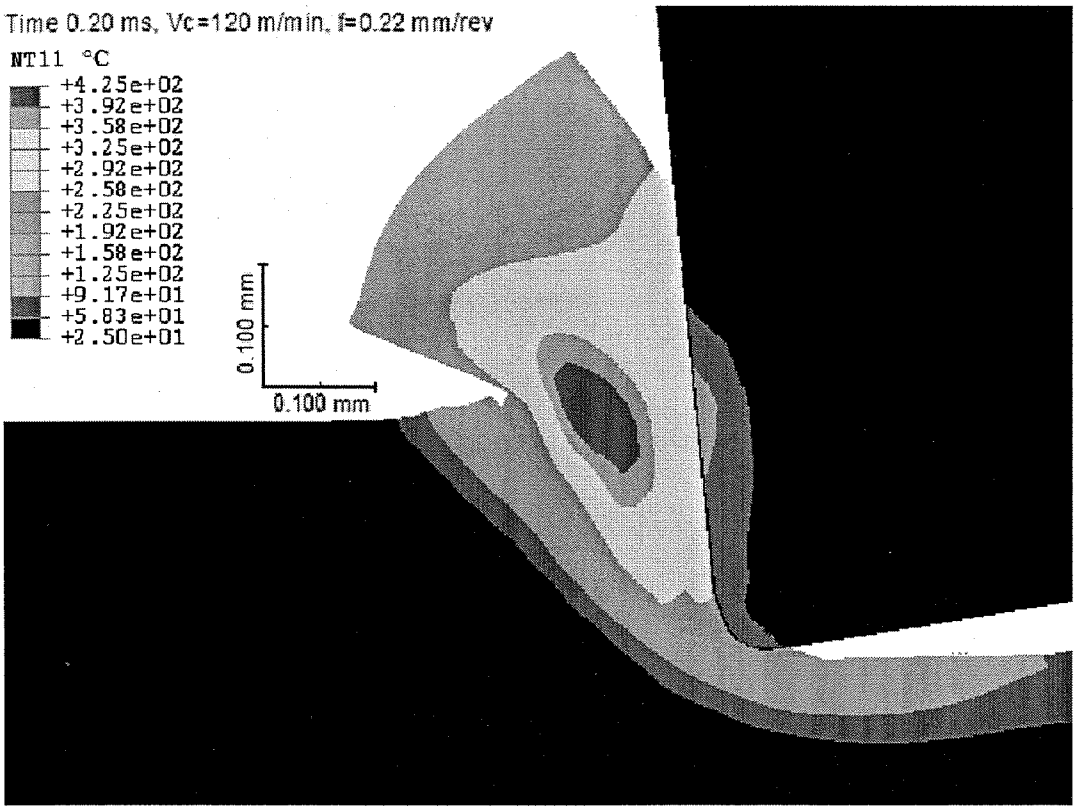

Figure 8: Temperature distribution simulation results with ABAQUS

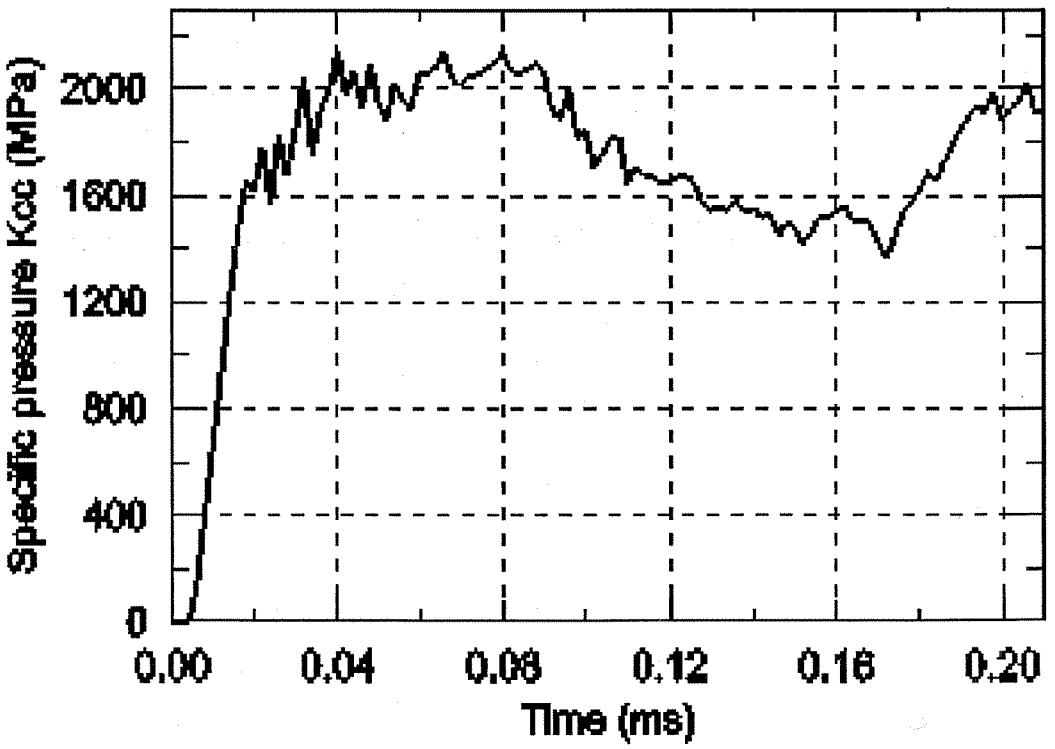

Figure 9: Specific cutting force as a function of time simulation results with ABAQUS

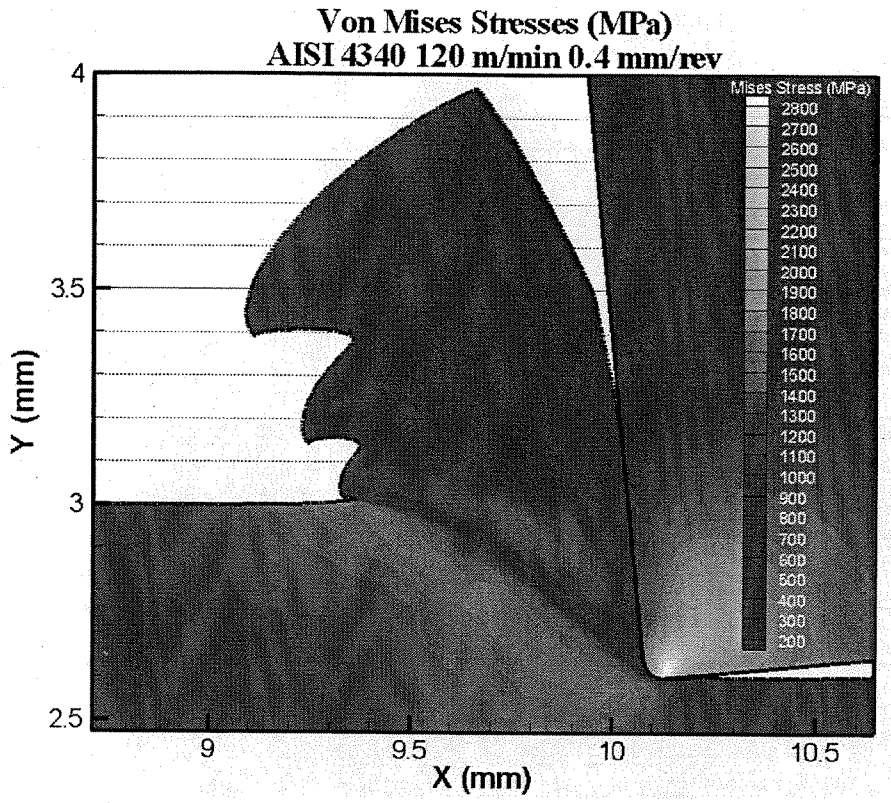

Figure 10: Von Mises stress profiles for 120 m/min cutting

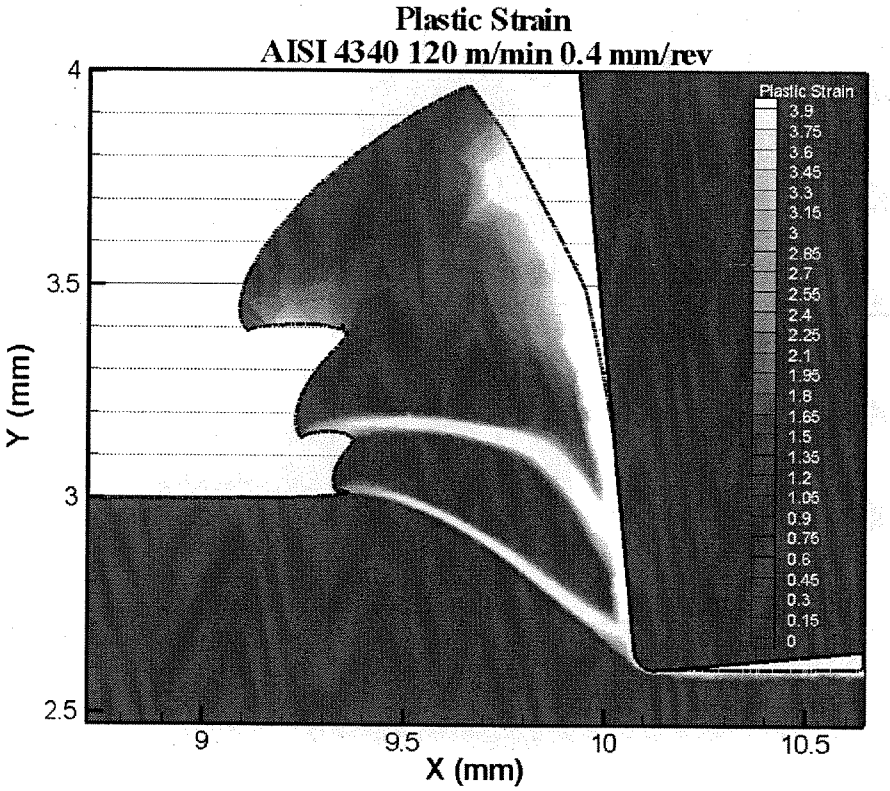

Figure 11: Plastic strain profiles for 120 m/min cutting

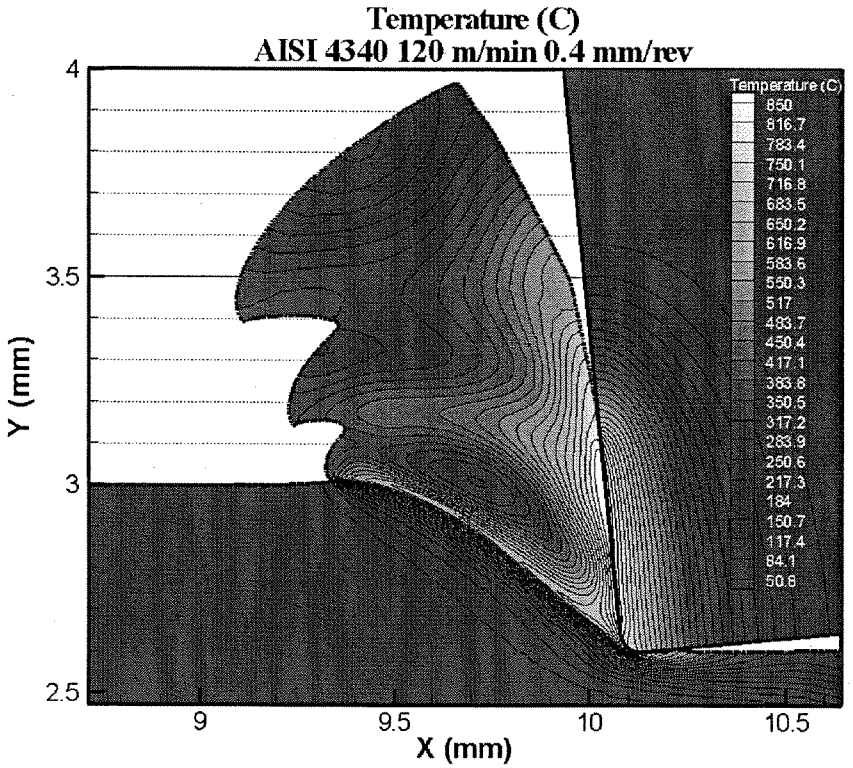

Figure 12: Temperature profiles for 120 m/min cutting speed

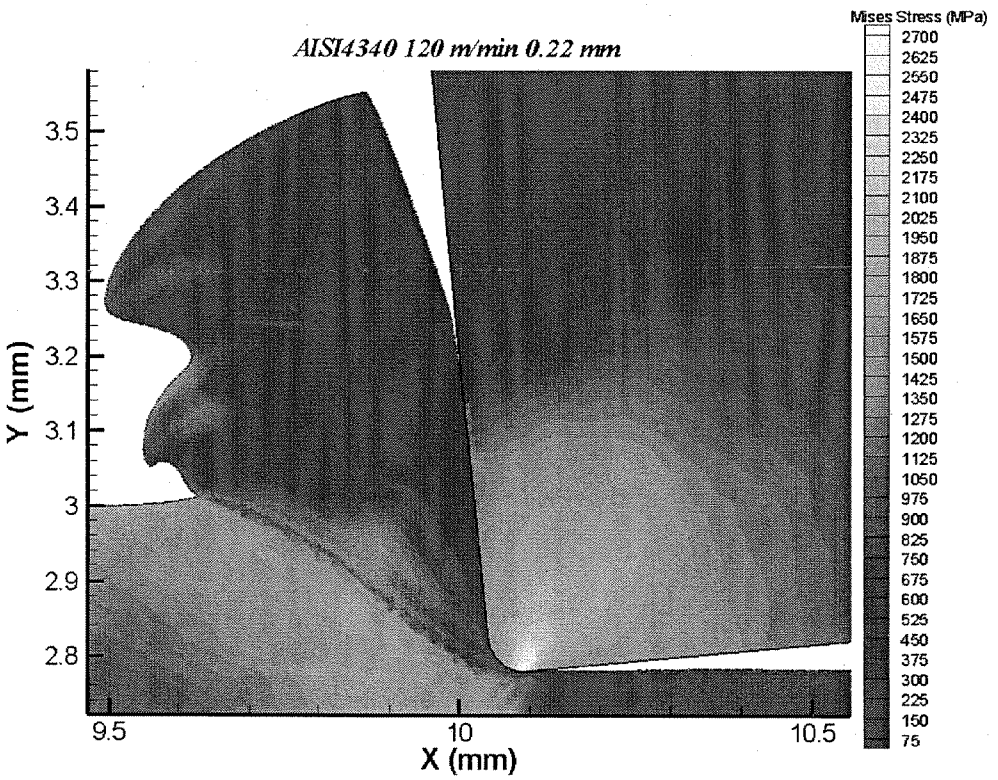

Figure 13: Von Mises stress profiles for 120 m/min cutting

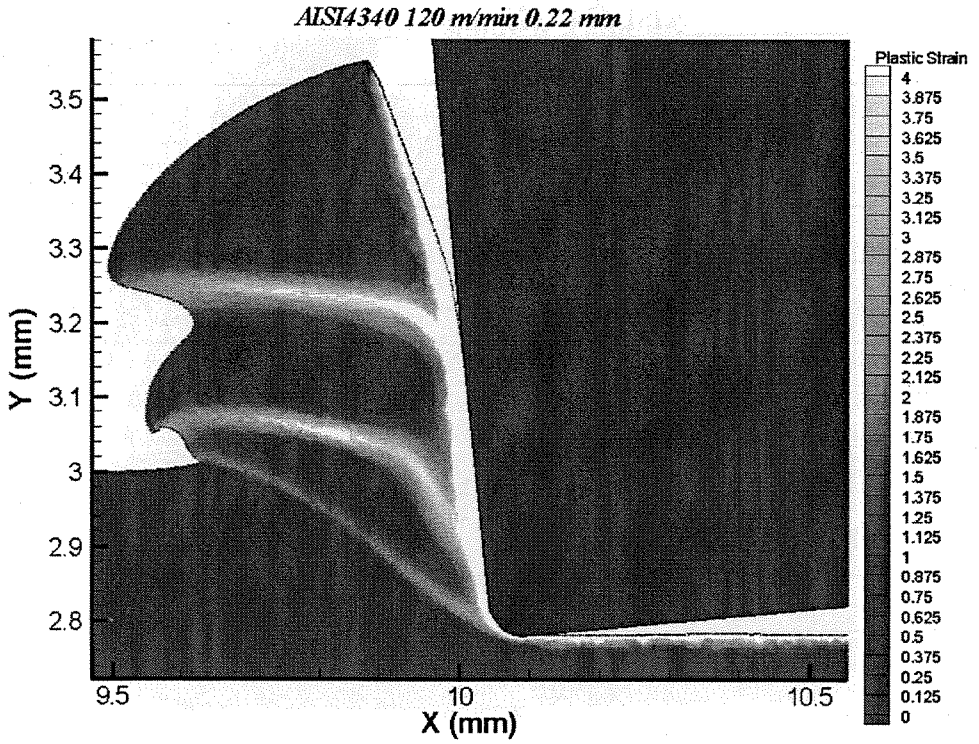

Figure 14: Plastic strain profiles for 120 m/min cutting speed

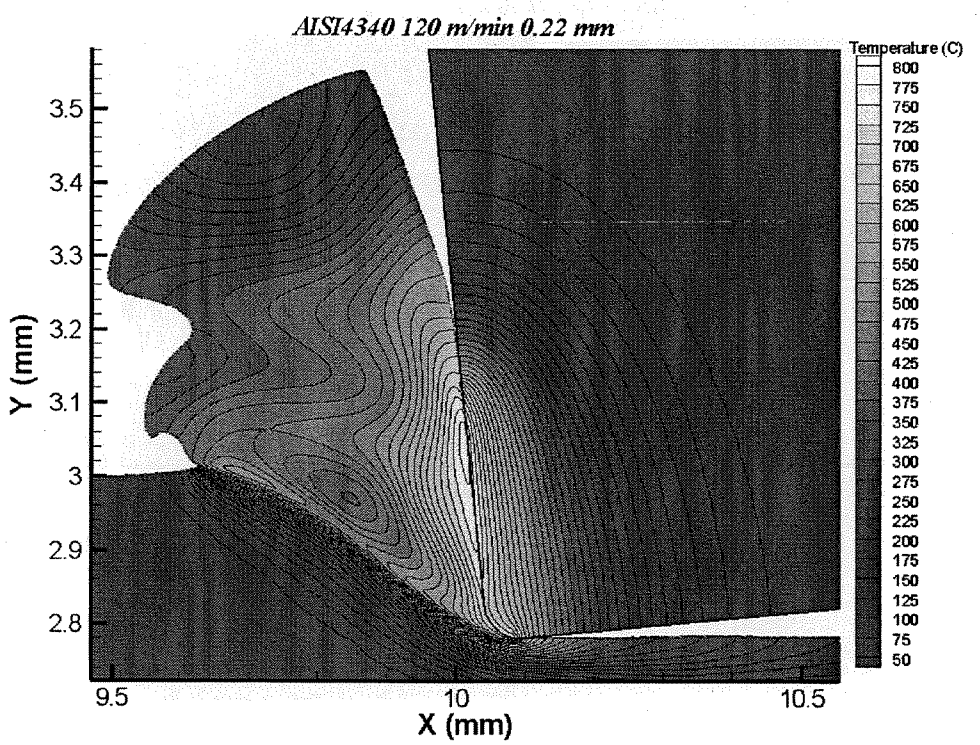

Figure 15: Temperature profiles for 120 m/min cutting speed